Advances in Science and Technology Research Journal

Advances in Science and Technology Research Journal, 2025, 19(1), 88–94
https://doi.org/10.12913/22998624/194603
ISSN 2299-8624, License CC-BY 4.0

Received: 2024.09.10
Accepted: 2024.11.15
Published: 2024.12.01

Time delay effect in double excited human middle ear

Robert Zablotni[1*], Weronika Dabrowa[2], Zofia Szmit[1], Rafal Rusinek[1]

[1] Department of Applied Mechanics, Lublin University of Technology, ul. Nadbystrzycka 36, Lublin, Poland
[2] Department of Agro-bioengineering, University of Life Sciences, ul. Akademicka 13, Lublin, Poland
* Corresponding author's e-mail: r.zablotni@pollub.pl

ABSTRACT

In the cases of significant hearing loss affecting the auditory ossicles, it is possible to attach an implant. In such cases, the implant is responsible for the movement of the stapes. However, the eardrum is not removed, it remains in the system, forcing movement of the first auditory ossicle – the malleus. The aim of this research was to present the results of stapes vibrations in the human ear with an implant under dual excitation both from the eardrum and the implant using Lumped Parameter Model with 5 degrees of freedom. The model incorporates the masses of all three auditory ossicles, as well as additional masses from the implant. The delay in the system caused by the signal reaching the implant is also considered. The results relate to the work that was later transformed into an ASTM standard for ear testing ensuring the accuracy of the findings.

Keywords: time delay, double excitation, ossicles, stapes vibration, implanted human middle ear.

INTRODUCTION

The auditory system is a great example of evolution [1], enabling humans to hear, which is crucial for communication, navigation, and awareness. The human ear, made up of the outer, middle, and inner ear, is designed to catch, boost, and change sound into signals that the brain can understand [2]. Sound starts its journey in the outer ear, which includes the pinna and ear canal. These parts direct sound waves to the eardrum, which is the entrance to the middle ear [2]. Inside the middle ear, tiny bones called ossicles—the malleus, incus, and stapes—work together to carry and amplify vibrations from the eardrum to the oval window, leading to the inner ear.

The inner ear, located in the temporal bone, contains the cochlea, vestibular system, and auditory nerve. The cochlea is essential for hearing [2]. It is a spiral-shaped, fluid-filled structure with special cells called hair cells. When sound vibrations reach the cochlea, they move the fluid, which in turn activates the hair cells to change mechanical energy into electrical signals. These signals travel through the auditory nerve to the brainstem and then to the brain's hearing centre [2]. The precision of human hearing is owing to the ear's detailed design and the complex processes that control it. Researchers use advanced models, like lumped parameter models, to study how the middle ear works [3–8]. These models simplify the middle ear into parts like masses, springs, and dampers, each with specific properties. They help understand things like how the ear's conduct, resonance frequencies, and energy transfer. These models are valuable for understanding hearing loss, designing hearing aids, and improving treatments. By studying middle ear mechanics, these models help advance the knowledge of hearing and create new solutions for hearing problems.

The middle ear implant (MEI) is a medical device that helps restore hearing in people with certain types of hearing loss. Unlike regular hearing aids that just amplify sound, these implants directly stimulate the ossicles or cochlea, bypassing the damaged parts of the ear. MEIs have three main parts: an external processor, a transducer, and an implanted receiver-stimulator [9]. The external processor picks up sound and changes it

into electrical signals. For ossicle stimulation, the signals are sent to a transducer on one of the ossicles, usually the incus. The transducer vibrates in response to the signals, bypassing the damaged parts and directly stimulating the functional parts to send sound (in form of vibration) to the inner ear. These implants improve sound quality, reduce feedback, and are more comfortable than traditional hearing aids, especially for those with certain types of hearing loss [9].

When placing an implant on the long or short process of the incus, one does not remove the tympanic membrane, regardless of its condition. This way (through the membrane), sound still reaches the ME ossicles causing movement and resulting in double stimulation. Furthermore, since the implant is an electronic system, it has a delay due to several factors, each contributing to the overall latency experienced in signal processing, communication, and computation. This research explored the double excitation phenomenon in implanted middle ears, using lumped parameter model to understand and explain the problem of MEI configuration and finally to improve hearing implants as well as their configuration. The reason for the double excitation test is the fact that, despite the deterioration of the hearing system, sound reaches the eardrum and sets it in motion despite the implant being placed on the incus. Consequently, ossicles are stimulated both by MEI and sound reaching to the tympanic membrane. This is a novel approach and important problem that has not been explored in the literature before.

The structure of the paper is organised as follows: Section 2 describes the model with an implant and the mathematical equations. Section 3 focuses on results from numerical simulation. Finally, Section 4 discusses the results and provides conclusions.

IMPLANTED HUMAN MIDDLE EAR MODEL

In the human middle ear, a chain of bones—the malleus, incus, and stapes—are connected each other by the incudomallear and incudostapedial joints [2]. This system of bones is also attached to the temporal bone with ligaments and tendons: the incus is secured by the posterior incudal ligament, and the malleus by the anterior mallear ligament. The stapes is linked to the oval window via the stapedial annular ligament. In an ear with an implant, a holder is usually placed on either the long or short process of the incus to support the system that induces movement [10].

In this model of the intact human middle ear (ME), visco-elastic properties of tendons and ligaments are represented by springs (k) and dampers (c). Experimental measurements of AL (Annular Ligament) stiffness are taken from [11] and are compared with the proposed cubic approximation in paper [12]. Three masses represent the ossicles: the malleus (m_M), the incus (m_I), and the stapes (m_S), that can move in the x direction on a base [5].

The floating mass transducer (FMT) includes a floating mass magnet (M_m) and a metal case (M_c). The magnet (M_m) is supported by dampers (c_m) and springs, which have both linear (km) and nonlinear components. The nonlinear parts include quadratic (k_{m2}) and cubic (k_{m3}) terms. Typically, silicone rubber is used as the suspension material for the magnet, and these parameters (k_{m2}, k_{m3}) describe the nonlinear properties of the silicone rubber, as reported in [13]. The floating mass in reality moves due to an electromagnetic field; however, in this case it is driven by an external force (P) with frequency (ω) which represents electromagnetic force between the magnet and a coil, as shown in Figure 1. FMT is attached to the short or to the long process of the incus and this connection is secured with a coupler (clip) that has damping coefficient c_{CLIP}, and linear and cubic stiffness coefficients k_{CLIP}, and k_{CLIP3}. The clip's stiffness is assumed as nonlinear (qubic – k_{CLIP3}) because can be adjusted for each patient if a specially designed coupler is used, e.g. coupler with variable stiffness published as a patent No. 238475 in Polish Patent Office [The Bulletin of the Patent Office 12/2021] Therefore, the differential equations governing the implanted human middle ear system in dimensional form are as follows:

$$\ddot{x}_M m_M + \tilde{k}_{11} x_M + \tilde{k}_{12} x_I + \tilde{c}_{11} \dot{x}_M + \tilde{c}_{12} \dot{x}_I = Q\cos(\omega t) \quad (1)$$

$$\ddot{x}_I m_I + \tilde{k}_{21} x_M + \tilde{k}_{22} x_I + \tilde{k}_{23} x_S + \tilde{k}_{24} x_C + \widetilde{+\gamma}_{24}(x_I - x_C)^3 + \tilde{c}_{21} \dot{x}_M + \tilde{c}_{22} \dot{x}_I + \tilde{+c}_{23} \dot{x}_S + \widetilde{+c}_{24} \dot{x}_C = 0 \quad (2)$$

$$\ddot{x}_S m_S + \tilde{k}_{32} x_I + \tilde{k}_{33} x_S + \tilde{c}_{32} \dot{x}_I + \tilde{+c}_{33} \dot{x}_S + \tilde{\gamma}_3 x_S{}^3 = 0 \quad (3)$$

$$\ddot{x}_C M_c + \tilde{k}_{42} x_I + \tilde{k}_{44} x_C + \tilde{k}_{45} x_m + \tilde{c}_{42} \dot{x}_I + \tilde{+c}_{44} \dot{x}_C + \tilde{c}_{45} \dot{x}_m - \tilde{\gamma}_{24}(x_I - x_C)^3 - \tilde{\beta}_{45}(x_C - x_m)^2 + \tilde{\gamma}_{45}(x_C - x_m)^3 = 0 \quad (4)$$

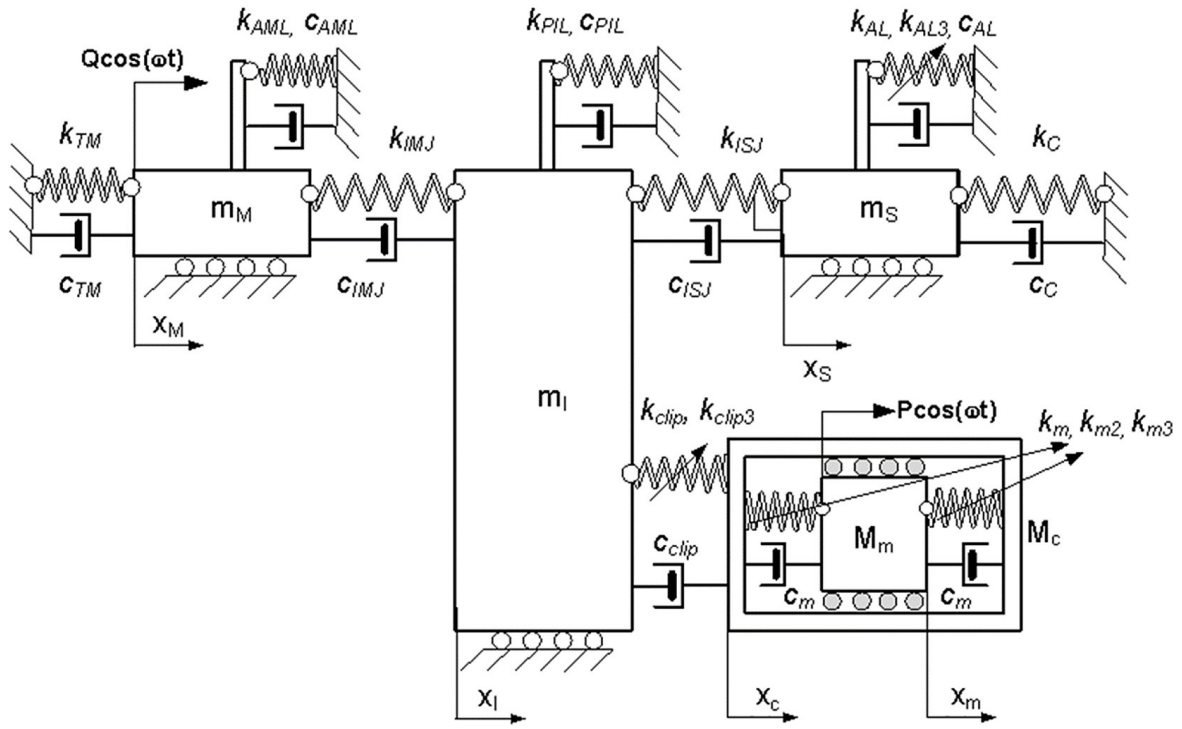

Figure 1. Lumped parameter model of implanted human middle ear with 5 degrees of freedom

$$\ddot{x}_M M_m + \tilde{k}_{54} x_C + \tilde{k}_{55} x_m + \tilde{c}_{54} \dot{x}_C + \tilde{c}_{55} \dot{x}_m + \tilde{\beta}_{45} (x_C - x_m)^2 - \tilde{\gamma}_{45} (x_C - x_m)^3 = H(\tau) * Pcos(\omega t) \quad (5)$$

where:

$$\begin{gathered} \tilde{k}_{11} = k_{TM} + k_{AML} + k_{IMJ}, \tilde{k}_{12} = -k_{IMJ}, \\ \tilde{c}_{11} = c_{TM} + c_{AML} + c_{IMJ} \\ \tilde{c}_{12} = -c_{IMJ}, \tilde{k}_{21} = \tilde{k}_{12}, \tilde{k}_{22} = \\ = k_{PIL} + k_{ISJ} + k_{IMJ} + k_{clip} \\ \tilde{k}_{23} = -k_{ISJ}, \tilde{k}_{24} = -\tilde{k}_{clip}, \tilde{\gamma}_{24} = \\ = k_{clip3}, \tilde{c}_{21} = -c_{IMJ}, \\ \tilde{c}_{22} = c_{PIL} + c_{ISJ} + c_{IMJ} + c_{clip}, \\ \tilde{c}_{23} = -c_{ISJ}, \tilde{c}_{24} = -c_{clip}, \\ \tilde{k}_{32} = \tilde{k}_{23}, \tilde{k}_{33} = k_{AL} + k_{ISJ} + k_C, \\ \tilde{c}_{32} = \tilde{c}_{23}, \tilde{c}_{33} = c_{AL} + c_{ISJ} + c_C, \tilde{\gamma}_3 = k_{AL3}, \\ \tilde{k}_{42} = \tilde{k}_{24}, \tilde{k}_{44} = k_{clip} + k_m, \tilde{k}_{45} = \\ = -k_m, \ \tilde{c}_{42} = \tilde{c}_{24}, \ \tilde{c}_{44} = c_{clip} + c_m, \\ \tilde{c}_{45} = -c_m, \tilde{\gamma}_{45} = k_{m3}, \tilde{\beta}_{45} = k_{m2}, \tilde{k}_{54} = \tilde{k}_{45} \\ \tilde{k}_{55} = k_m = -\tilde{k}_{54}, \tilde{c}_{54} = \tilde{c}_{45}, \tilde{c}_{55} = c_m = -\tilde{c}_{54} \end{gathered} \quad (6)$$

In this model, it is assumed that the excitation *P* applied to the FMT would be delayed, as delays are common in electronic systems. Then, Heaviside step function *H(τ)* is defined as follows:

$$H(\tau) = \begin{cases} 0 \ for \ t < \tau \\ 1 \ for \ t \geq \tau \end{cases} \quad (7)$$

where: *t* means delay of the FMT due to electronic equipment.

RESULTS AND ANALYSIS

Numerical simulations of the model presented in Section 2 are compared with experimental outcomes reported in ASTM standard [14] concerning Standard Practice for Describing System Output of Implantable Middle Ear Hearing Devices. The analysis is focused significantly on the stapes vibration because of its pivotal role in facilitating sound transmission to the inner ear. Hence, the configuration and operation of the implant are critically important from the end user's standpoint.

Methodology

The middle ear transfer function (METF), classically used for estimation of stapes vibration will be compared with experimental data taken from [14, 15]. The METF indicates stapes displacement divided by sound pressure versus excitation frequency produced by sound stimulation or/and the FMT. According to the ASTM standard, the METF, measured in an experiment on temporal bone, should meet the criterion defined by Rosowski et al. in 2007 [15]. Later, the criterion becomes the basis for the ASTM standard [14] concerning measurement accuracy in the middle ear which is presented graphically as

Table 1. Parameters for 5DOF lumped parameter model

Name	Abbr.	Value
Tympanic memebrane stiffness parameter	k_{tm}	300 [N/m]
Anterior mallear ligament stiffness parameter	k_{aml}	800 [N/m]
Incudomallear joint stiffness parameter	k_{imj}	1000000 [N/m]
Posterior incudal ligament stiffness parameter	k_{pil}	400 [N/m]
Incudostapedial joint stiffness parameter	k_{isj}	1350 [N/m]
Cochlea stiffness parameter	k_c	200 [N/m]
Annular ligament stiffness parameter	k_{al}	623 [N/m]
Cubic nonlinear stiffness parameter of the annular ligament	k_{al3}	1.3e+13 [N/m]
Stiffness parameter of the mas inside the FMT	k_m	850 [N/m]
Square nonlinear stiffness parameter of the mas inside the FMT	k_{m2}	1.88e+8 [N/m]
Cubic nonlinear stiffness parameter of the mas inside the FMT	k_{m3}	1.4e+13 [N/m]
Stiffness parameter of the clip of the FMT	k_{clip}	20000 [N/m]
Cubic nonlinear stiffness parameter of the clip of the FMT	k_{clip3}	2.25e+15 [N/m]
Tympanic membrane dumping parameter	c_{tm}	0.06 [Ns/m]
Tympanic membrane dumping parameter	c_{aml}	0.275 [Ns/m]
Anterior mallear ligament dumping parameter	c_{imj}	0.359 [Ns/m]
Incudomallear joint dumping parameter	c_{pil}	0.055 [Ns/m]
Posterior incudal ligament dumping parameter	c_{isj}	0.0079 [Ns/m]
Incudostapedial joint dumping parameter	c_c	0.0017 [Ns/m]
Annular ligament dumping parameter	c_{al}	0.0020 [Ns/m]
Damping parameter of the mas inside the FMT	c_m	0.32 [Ns/m]
Damping parameter of the clip of the FMT	c_{clip}	0.15 [Ns/m]
Malleus mass	m_M	2.5e-5 [kg]
Incus mass	m_I	2.8e-05 [kg]
Stapes mass	m_S	1.78e-06 [kg]
Floating mass	M_m	1e-5 [kg]
FMT case mass	M_c	1.5e-5 [kg]
Mechanical excitation force applied to the FMT	P	4.32e-05 [N]
Mechanical excitation force applied to the first mass	Q	3.336e-05 [N]

a grey region in Figure 2. Numerical simulations are developed using MATLAB Simulink using the mathematical models defined by Equations 1–5. These simulations employ the Runge-Kutta 4th order method (ode45) with a variable step size and a relative tolerance of 10-10 s for accurate computations. The numerical experiments utilised the parameters listed in Table 1. Stiffness (k), damping (c), and mass (m) parameters were derived from [8], while additional parameters introduced in the model are estimated based on experimental data.

Numerical simulations were performed in three variants, namely as sound stimulation (Q), FMT stimulation (P) and simultaneously sound and FMT force stimulation ($Q + P$) with various time delay (τ).

Numerical results

Figure 2a presents three curves obtained from numerical simulations of the model presented in the previous section. It can be observed that for double excitation with P and Q as mentioned in Table 1 without time delay, the blue curve lies within the range indicated in the literature up to frequencies around 4 kHz. When the excitation is applied only to the FMT (P), the METF value is low but still falls within the literature range. For excitation applied only to the first bone (sound stimulation of the TM with the force Q) in the implanted ear, METF values are also small and the lowest and around 850-1000 Hz. Moreover, it drops down below the range indicated in [15] (grey area in Figure 2).

In this study, it was assumed that the excitation P applied to the FMT would be delayed, as delays are common in electronic systems. Figure 2b shows METF with delays of 0.01 s, 0.03 s, and 0.05 s. All of these curves have a drop, at 4 kHz, 2.2 kHz and 1.5 kHz, respectively from the smallest to the largest delay time. The curves with a time delay of 0.03 s and 0.05 s have the best fit to the literature and ASTM criterion.

In Figure 2c, three curves are shown for smaller delay times of 0.001 s, 0.003 s, and 0.005 s. For t delay time t = 0.005 s – the green curve – METF has the best fit to literature criterion and has only one drop around 1.5 kHz. For the curves with delay times of 0.001 s and 0.003 s, there are cyclic increases and decreases in METF values. Both of those curves (black and blue) fall below literature criterion at 0.5 kHz and 1.6 kHz. However, for the higher delay time (blue curve), the curve returns to the range in lower frequency range than the black curve. For both of these curves (black and blue), cyclic increases and decreases in amplitude are observed which will be explained in next chapter.

In the case of even smaller delay, presented in Figure 2d, the curve with the shortest delay time of 0.0005 s shows the best fit to the literature range of METF (it is below range only around 1kHz and 2.1 kHz). For a delay time of 0.0003s, the curve (blue) drops below the range for frequencies around 100 Hz, 900 Hz,1400 Hz and 2400 Hz. For a delay time of 0.0001 s, the black curve drops below in three areas, first from around 450 Hz to 650 Hz, second from 1.5 kHz to 1.6 kHz and third around 2.7 kHz.

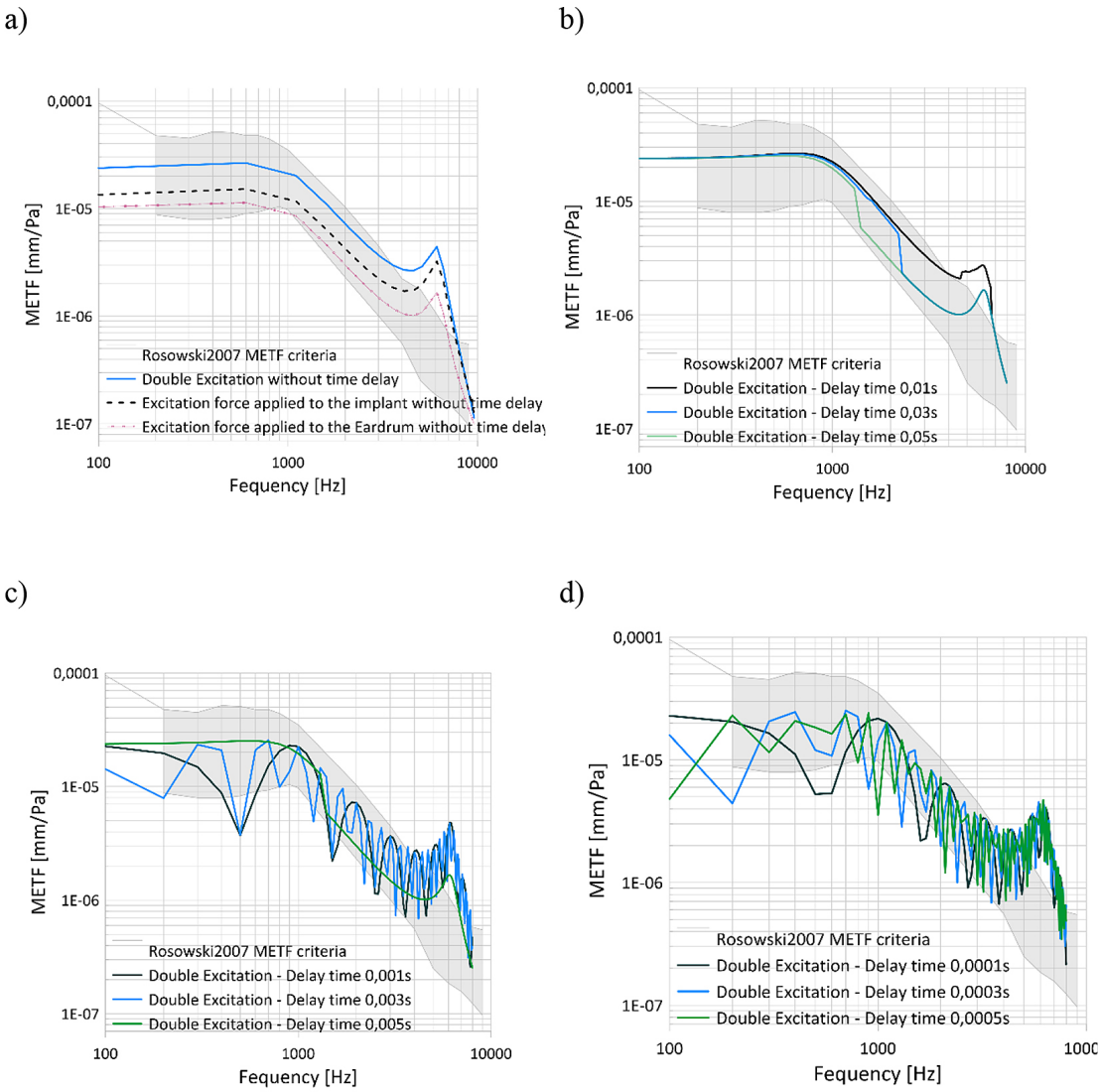

Figure 2. Middle ear transfer function comparison between numerical results and Rosowski et al. 2007 [15] (ASTM standard [14]). Single excitations without time delay effect (a), double excitation with different times of delay (b–d)

RESULTS AND DISCUSSION

To explain the effect of double excitation and time delay, an amplitude of stapes vibration (a_3) for 1 kHz excitation frequency is shown in Figure 3, which illustrates how the amplitude of stapes vibration (a_3) changes with time delay (τ). There are cyclic increases and decreases in the amplitude values depending on τ. The period of change in the amplitude (a_3) of vibrations caused by the delay is $T = \frac{1}{1000}\,s$ which is marked in the figure. Three points (A, B, C) are marked and their meaning is explained in Figure 4.

In Figure 4, three periodic forces are depicted: the excitation force on the malleus coming from sound stimulation (q), the excitation force of the FMT (p), and their sum (p+q). The mentioned forces are dimensionless in the simulation calculated as $q = \frac{Q}{m_M \cdot x_{st} \cdot \omega_0^2}$ and $p = \frac{P}{m_M \cdot x_{st} \cdot \omega_0^2}$, where x_{st} = 1 mm and $\omega_0 = \sqrt{\frac{k_{aml}}{m_M}}$ just to fasten simulations Figure 4a, which corresponds to the point A on the amplitude plot from Figure 3, shows that both forces are in phase because delay (τ) is equal to the excitation period (or multiple of excitation period $\frac{2\pi}{\omega}$), resulting in the largest combined force. Figure 4b illustrates the forces at a point B indicated in Figure 3 between the maximum and minimum values where a phase shift coming from delay between the forces leads to a smaller resultant force than in Figure 4a. Figure 4c displays the forces at the lowest point on the amplitude graph (Figure 3), where the forces are in opposite phases, yielding the smallest sum (p + q). This significantly impacts the amplitude graph in Figure 3 and also influences the oscillations observed in Figures 2b–d, where the METF results from the forces summing in different phases due to a constant time delay and varying excitation frequency. If time delay meets excitation period, stapes vibration is amplified, whereas delay is half of the excitation period, vibration is reduced significantly.

The literature lacks analyses of double excitation problem in the implanted ear stimulated by FMT despite some experimental results reveal fluctuations in METF, as seen in Shraven et al. [16] and Shin et al. [17]. These experimental works [16, 17] in which the stapes movements

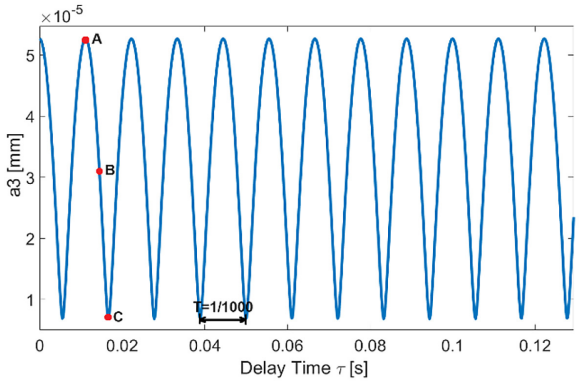

Figure 3. Changes in amplitude of the stapes vibration depending on the excitation force delay time (τ) for 1 kHz

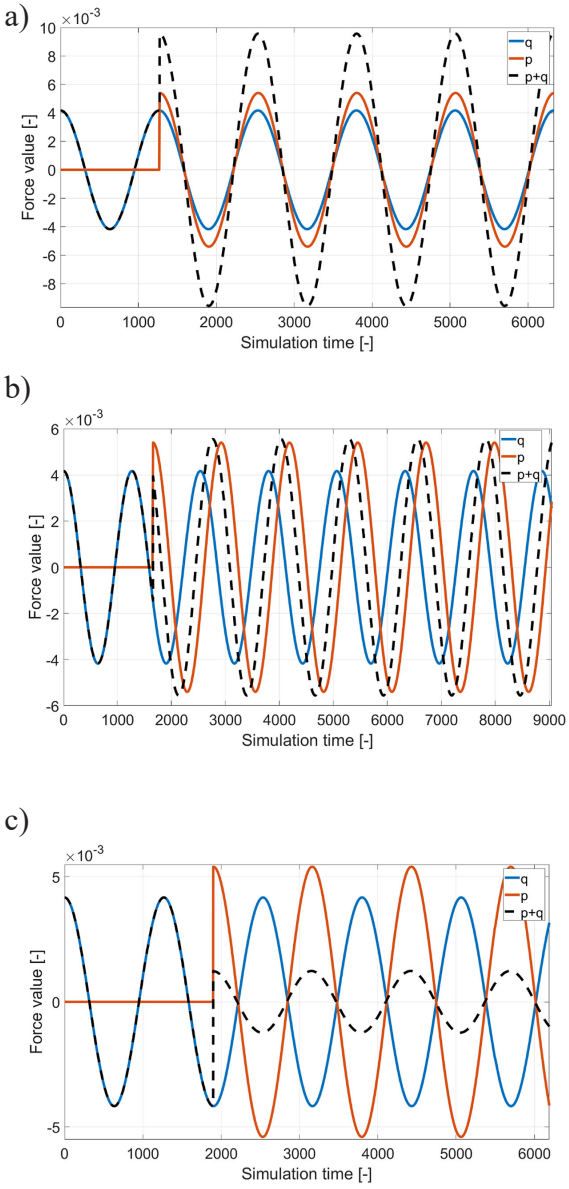

Figure 4. Plot of the sinusoidal excitation forces on the malleus from sound stimulation (p), from FMT (p) and sum of both excitation forces (p + q) for points A,B and – indicated in Figure 3, respectively

forced by the FMT are analysed, show that METFs are not smooth as in the numerical and experimental results obtained for unaided ear (without FMT). It is therefore expected that the fluctuations are caused by the double excitation and the delay in the action of one of the two excitation sources. Unlike studies [4, 8], the results obtained from the model under investigation does not display nonlinear phenomena. Stapes vibration always is regular.

Considering Figures 2–4, it is crucial to account for potential delays in the system when configuring the implant. These delays can significantly affect implant performance, particularly during double excitation, which may introduce disturbances like amplitude fluctuations that fall below the METF accepted range, as noted in [15]. These findings are important, because they directly impact the reliability and precision of sound transmission in middle ear implants. In real-world applications, accurately addressing these delays is essential for optimising the implant's performance, improving the clarity and stability of sound perception for users. By minimising the disturbances caused by delays, implant devices can better align with natural auditory processes, ultimately leading to more consistent and effective hearing restoration for patients. This optimisation can enhance user satisfaction, reduce complications, and improve long-term auditory outcomes.

Acknowledgements

The research was financed in the framework of the project no. 2022/45/N/ST8/02447, funded by the National Science Centre, Poland as well as IDeaS of LUT - NAWA STER.

REFERENCES

1. Hachmeister J.E. An abbreviated history of the ear: from Renaissance to present. Yale J Biol Med. 2003, 76(2), 81–6. PMID: 15369636; PMCID: PMC2582694.
2. Bruss D.M., Shohet J.A. Neuroanatomy, Ear. 2023 Apr 3. In: StatPearls [Internet]. Treasure Island (FL): StatPearls Publishing; 2024 Jan–. PMID: 31869122.
3. Zwislocki J. Analysis of the Middle-Ear Function. Part I: Input Impedance. J. Acoust. Soc. Am. 1962, 34, 1514–1523.
4. Rusinek R., Lenci S. Stapes vibrations induced by piezoelectric floating mass transducer. Journal of Sound and Vibration, Volume 548, 117556, 2023.
5. Rusinek R., Szymanski M., Zablotni R. Biomechanics of the Human Middle Ear with Viscoelasticity of the Maxwell and the Kelvin–Voigt Type and Relaxation Effect. Materials. 2020, 13(17), 3779.
6. Rusinek R., Warminski J., Szymanski M., Kecik K., Kozik K. Dynamics of the middle ear ossicles with an SMA prosthesis. Int. J. Mech. Sci. 2017, 127, 163–175.
7. Rusinek R., Kecik K. Effect of linear electromechanical coupling in nonlinear implanted human middle ear. Mechanical Systems and Signal Processing 2021, 151, 107391.
8. Rusinek R. Sound transmission in the first nonlinear model of middle ear with an active implant. Math. Probl. Eng. 2020, 2020, 4580467.
9. MED-EL, website, www.medel.pro
10. Luers J.C., Hüttenbrink K.B. Surgical anatomy and pathology of the middle ear. J Anat. 2016 Feb, 228(2), 338–53.
11. Lauxmann M., Eiber A., Haag F., Ihrle S. Nonlinear stiffness characteristics of the annular ligament. J. Acoust. Soc. Am. 2014, 136, 1756–1767.
12. Rusinek R. sound transmission in the first nonlinear model of middle ear with an active implant. Mathematical Problems in Engineering, 2020, 4580467.
13. Darvish B., Najarian S., Shirzad E., Khodambash R. A novel tactile force probe for tissue stiffness classification. American Journal of Applied Sciences, 2009, 6(3), 512–517.
14. Standard Practice for Describing System Output of Implantable Middle Ear Hearing Devices. ASTM F2504-05 (Reapproved 2022).
15. Rosowski J.J., Chien W., Ravicz M.E., Merchant S.N. Testing a method for quantifying the output of implantable middle ear hearing devices. Audiol Neurootol. 2007, 12(4), 265–76.
16. Schraven S. P., Mlynski R., Dalhoff E., Heyd A., Wildenstein D., Rak K., Radeloff A., Hagen R., Gummer A. W., Coupling of an active middle-ear implant to the long process of the incus using an elastic clip attachment, Hearing Research 2016, 340, 179–184.
17. Shin D. H., Seong K. W., Nakajima H. H., Puria S., Cho J. H. A piezoelectric bellows round-window driver (PBRD) for middle-ear implants. IEEE Access, 2020, 8, 137947–137954.